Data set from long-term wave, wind and response monitoring of the Bergsøysund Bridge

Knut Andreas Kvåle[1*], Aksel Fenerci[2], Øyvind Wiig Petersen[1], Anders Rønnquist[1], Ole Øiseth[1]

[1]Norwegian University of Science and Technology, NTNU, Faculty of Engineering, Department of Science and Technology, Trondheim, Norway

[2]Norwegian University of Science and Technology, NTNU, Faculty of Engineering, Department of Ocean Operations and Civil Engineering, Ålesund, Norway

Abstract

Wind, wave, displacement and acceleration data have been collected in a measurement campaign on the Bergsøysund Bridge, an end-supported pontoon bridge, between the years 2014 and 2018. The data set is now available in an open-access research entry published on Zenodo, for free access and download. The data are collected in two h5-files (hierachical data format), with sampling rates 2 Hz and 10 Hz, downsampled from the raw sampling rate of 200 Hz. Note that the data has undergone some minimal signal processing and adjustment. Some examples of how to import and browse through the data using an openly available Python package are also given.

1 Introduction

Experimental data of large bridges are often collected as a part of structural health monitoring. The data are not very commonly made publicly available, even though it may have large potential for use in numerous scientific applications. Consequently, the structural measurement data of these structures are in high demand. Some examples of available measurement data of bridges are Fenerci et al. (2021); Johnson et al. (2004); Kvåle et al. (2022b); Maeck and De Roeck (2003); Maes and Lombaert (2021); Wernitz et al. (2021). As floating bridges are rare, openly accessible global response and excitation data do not presently exist. Data applicable to dynamic study are therefore highly valuable for gaining insight into their behavior. Furthermore, long-span floating bridges are flexible and lively structures with a complicated dynamic behavior. Therefore, in addition to enabling improvement of future floating bridge designs, the data also have a more generic scientific value.

This paper describes the openly available database resulting from the monitoring of the Bergsøysund Bridge in Norway. The Bergsøysund Bridge is the second longest end-supported pontoon bridge in the World. We recently also published a similar dataset obtained from the monitoring of the Hardanger Bridge (Fenerci et al., 2021) and the Gjemnessund Bridge (Kvåle et al., 2022b). As part of the Coastal Highway E39 project led by the Norwegian Public Roads Administration (NPRA), where floating bridges are considered as viable solutions for many of the crossings to replace the current ferry connections, several aspects of the floating Bergsøysund Bridge have been studied in the last decade (Kvåle et al., 2016; Kvåle and Øiseth, 2017; Kvåle et al., 2017; Kvåle and Øiseth, 2019, 2021a,b; Petersen and Øiseth, 2017; Petersen et al., 2018, 2019). A crucial part of the studies has been the collection and analysis of experimental data on the environmental actions on and structural response of the bridge. Consequently, a large amount of data have been gathered during the measurement campaign. The data are now made available for open access on the online repository Zenodo (Kvåle et al., 2022a), and the current paper describes the major aspects of the data set. This includes descriptions of the data hierarchy, metadata, monitoring system, and examples for import and retrieval of the data.

Preprint Published version available at ascelibrary.org: *10.1061/JSENDH/STENG-12095*

Figure 1. Photograph of the Bergsøysund Bridge. Photo: NTNU/K.A. Kvåle.

2 Site description

The Bergsøysund Bridge, shown in Figure 1, is located on the western coast of Norway and was opened to traffic in 1992. Structural drawings of the bridge are shown in Figure 2. The geographic location of the bridge is depicted in Figure 3. At the time of opening, it was the longest floating bridge without side-anchoring in the World. It is still a unique structure, and its simple and symmetric geometry makes it an ideal case study for measurement campaigns, with potential of large transferable value to other floating bridges. The Norwegian west coast is also typically exposed to harsh winds and waves. The bridge stretches 930 meters in total, with a floating span of 830 meters, between the islands of Aspøya and Bergsøya, near Kristiansund in Møre og Romsdal county.

3 Monitoring system

Figure 4 depicts the main sensor layout of the monitoring system, consisting of 14 triaxial accelerometers, six wave radars, five ultrasonic anemometers and a global navigation satellite system (GNSS) displacement sensor. The precise coordinates of all sensors are provided digitally in the shared database, listed in Table 1 and illustrated in Figure 5. The sensor types and specifications are summarized in Table 2. Photographs of all sensor types are shown in Figure 6. Each pontoon has a separate logger unit connected to several nearby sensors by ethernet cable, which furthermore communicates with a main logger unit via WiFi. The data from the loggers are synchronized by GPS antennae. The data are resampled to 200 Hz before transmission to the main logger for storage. For more details on the measurement system and the bridge, it is referred to Kvåle and Øiseth (2017).

3.1 Revision history

Several revisions to the sensor layout have been made throughout the campaign, as access to new sensors or new applications have emerged. The revision history of the sensor layout is summarized in Table 3. It is noted that some of the anemometers were mounted slightly skewly (maximum 5 degrees off) in the period 2015/03/25–2015/09/28,

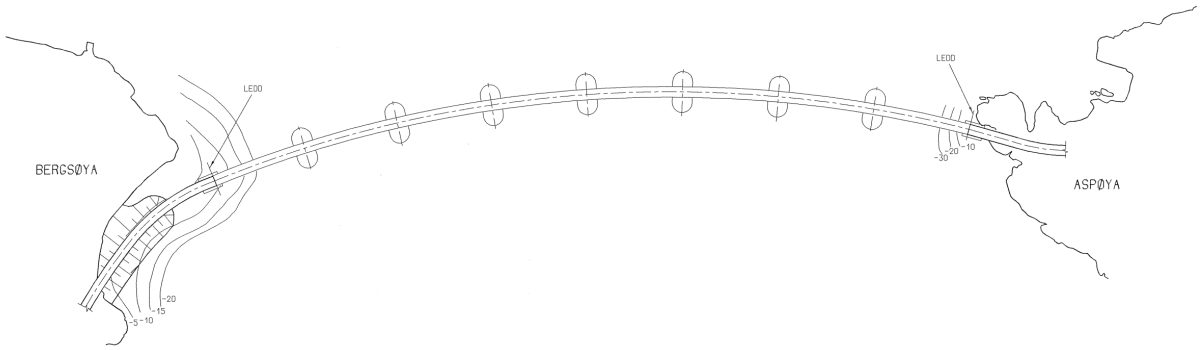

(a)

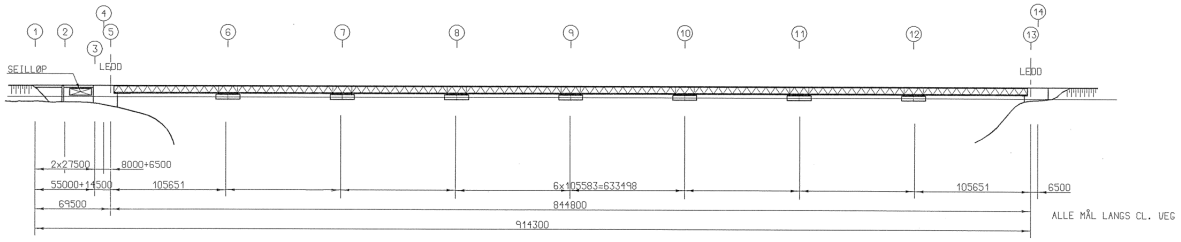

(b)

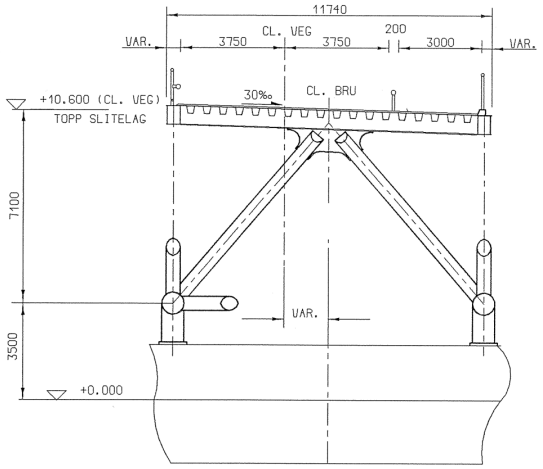

(c)

Figure 2. Structural drawings of the Bergsøysund Bridge. Drawings by Vegdirektoratet/Veritec/Johs Holt. (a) Plan, (b) Elevation, (c) Cross section.

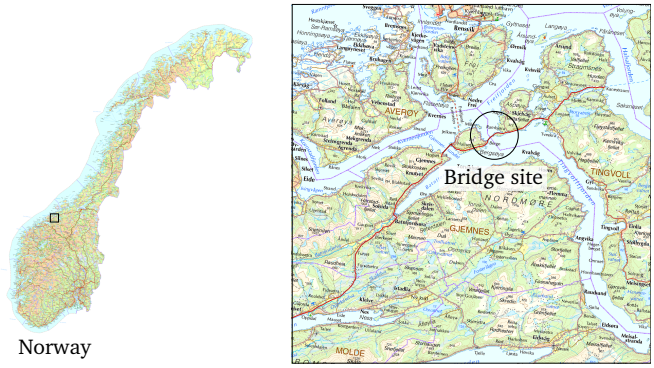

Figure 3. Map section showing location of the Bergsøysund Bridge. Maps: ©Kartverket.

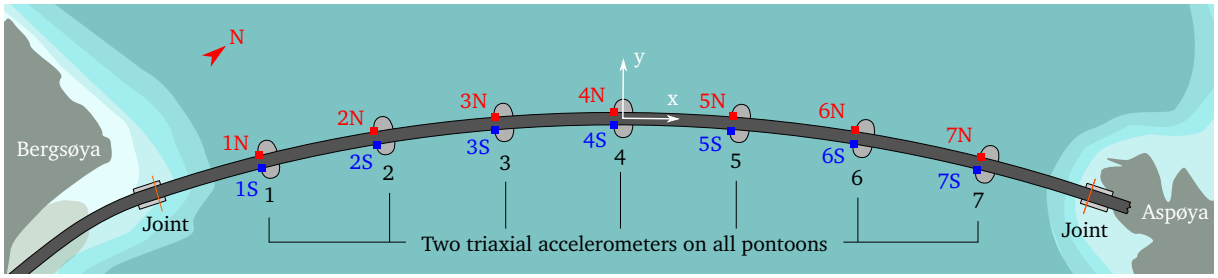

(a)

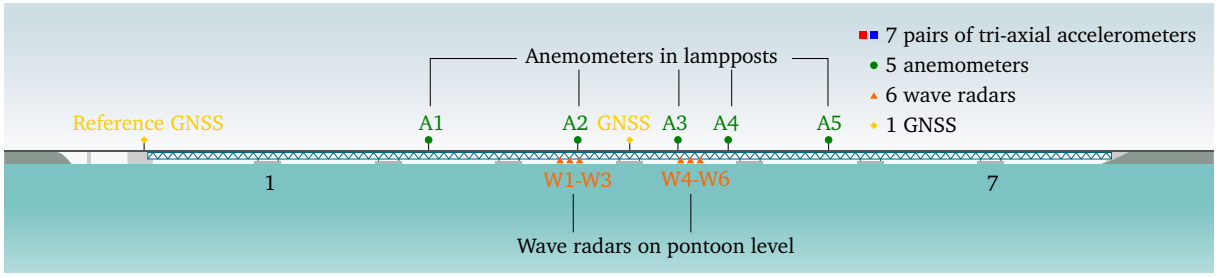

(b)

Figure 4. Monitoring system (layout Main) on the Bergsøysund Bridge (Kvåle and Øiseth, 2017). Reproduced with permission from Elsevier. (a) Top view, (b) Side view.

Table 1. Sensor positions in global coordinates.

		Position		
Sensor group	Sensor	x [m]	y [m]	z [m]
Accelerometers	1S	-318.99	-44.18	-7.00
	1N	-321.26	-35.90	-7.00
	2S	-216.35	-22.59	-7.00
	2N	-217.83	-13.92	-7.00
	3S	-112.21	-9.42	-7.00
	3N	-113.01	-0.35	-7.00
	4S	-7.21	-4.57	-7.00
	4N	-7.27	4.53	-7.00
	5S	97.74	-8.24	-7.00
	5N	98.42	0.83	-7.00
	6S	202.22	-20.28	-7.00
	6N	203.49	-11.57	-7.00
	7S	305.34	-40.79	-7.00
	7N	307.30	-32.42	-7.00
Anemometers	A1	-175.47	-6.25	8.00
	A2	-43.99	4.86	8.00
	A3	43.99	4.86	8.00
	A4	87.93	2.64	8.00
	A5	175.47	-6.25	7.50
GPS sensor	GNSS	0.00	-5.60	2.00
Wave radars (Main)	W1	-72.96	-1.39	-6.16
	W2	-52.99	-0.41	-6.16
	W3	-33.00	0.24	-6.16
	W4	33.00	0.24	-6.16
	W5	52.99	-0.41	-6.16
	W6	72.96	-1.39	-6.16
Wave radars (Alternative)	W1b	-72.96	-1.05	-6.16
	W2b	-71.86	-2.65	-6.16
	W3b	-69.67	-1.21	-6.16
	W4b	-64.17	-2.25	-6.16
	W5b	-52.19	-0.39	-6.16
	W6b	-29.13	-0.99	-6.16

Table 2. Sensor specifications.

Sensor type	Sensors	Model	Sample rate	Description
Accelerometer	1S–7S, 1N–7N	Canterbury Seismic Instruments CUSP-3	200 Hz	Triaxial MEMS accelerometer
Anemometer	A0–A5	Gill Instruments WindMaster Pro	32 Hz	Ultrasonic 3D anemometer
GNSS displacement sensor	GNSS	Trimble RTK GNSS	20 Hz	Real-time kinematics (RTK) GNSS sensor with reference sensor to adjust for disturbances
Wave radar	W1–W6, W1b–W6b	Miros SM-140 Range Finder	50 Hz	Triangular Frequency Modulated Continuous Wave microwave sensor, that provides single point measurements of distance to sea surface

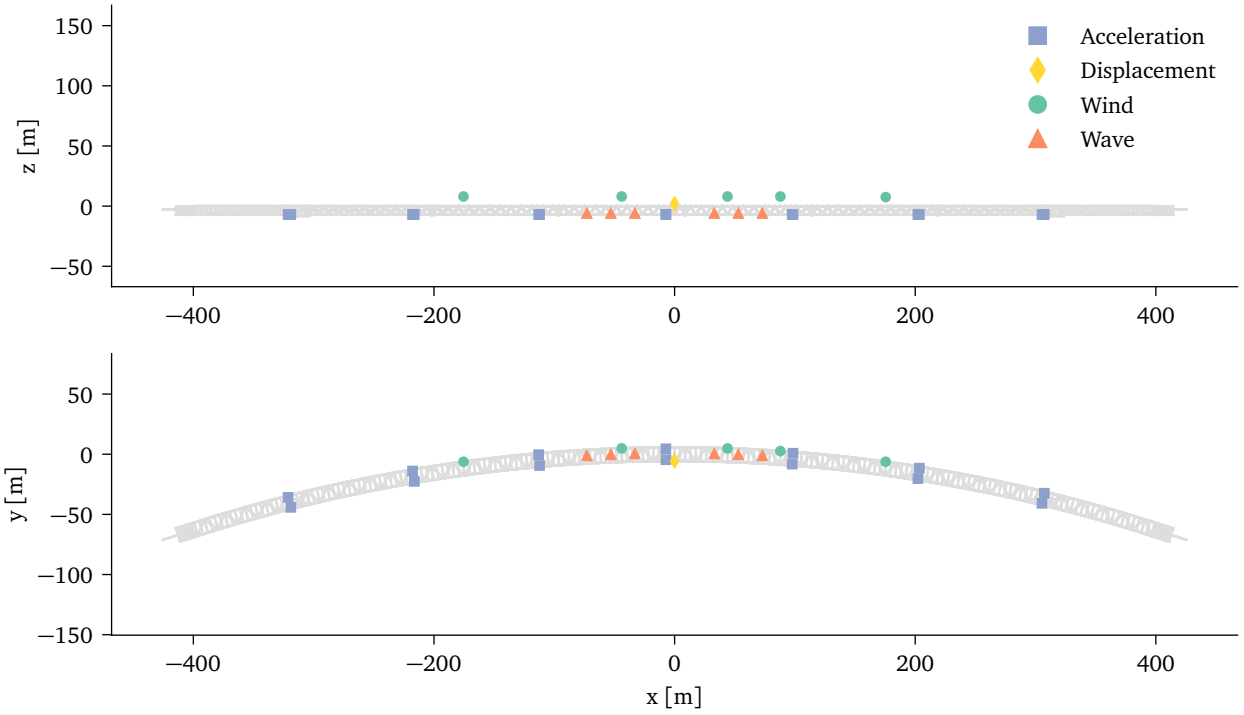

Figure 5. Sensor positions and shaded beam element model. The exact numerical coordinates are available as metadata in the shared database.

but were corrected through transformation matrices corresponding to the measured angles. Also, anemometer A3 needed to be changed during sensor layout revision *Main* due to damage (see Figure 7).

3.1.1 Rearranging wave radars

Initially, the monitoring system was designed to study wave correlation and potential inhomogeneity, and not to characterize the directionality of the sea state. In the last revision of the monitoring system, the positions of the wave radars were adjusted to enable optimal estimation of both of frequency and directional distributions of the wave field. Goda (1981) provided guidelines for the design of arrays of wave buoys (or wave radars) for the estimation of directional spectral densities of waves. They are based on the distance vectors between pairs of wave radars, $\{\mathbf{\Delta r}_{ij}\}$, and can be summarized as follows:

Table 3. Sensor layout history. Anemometer A0 which was part of the *Basic* sensor layout had a temporary sensor location only used during this stage, underneath the bridge deck. Its recordings are therefore highly affected by the surrounding truss and water surface, but included in the database regardless, as it might provide some useful insight for interpreting the corresponding wave data. Wave radars with suffix *b* (in layout *Alternative*) refer to new locations, as described in Section 3.1.1.

Layout	Period	Sensors			
		Acceleration	Wind	Wave elevation	Displacement
Preliminary	–2014/12/06	2S–6S and 2N–6N	-	-	-
Basic	2014/12/07–2015/03/24	1S–7S and 1N–7N	A0	W1–W6	-
Main	2015/03/25–2017/05/30	1S–7S and 1N–7N	A1–A5	W1–W6	GNSS
Alternative	2017/05/31–	1S–7S and 1N–7N	A1–A5	W1b–W6b	GNSS

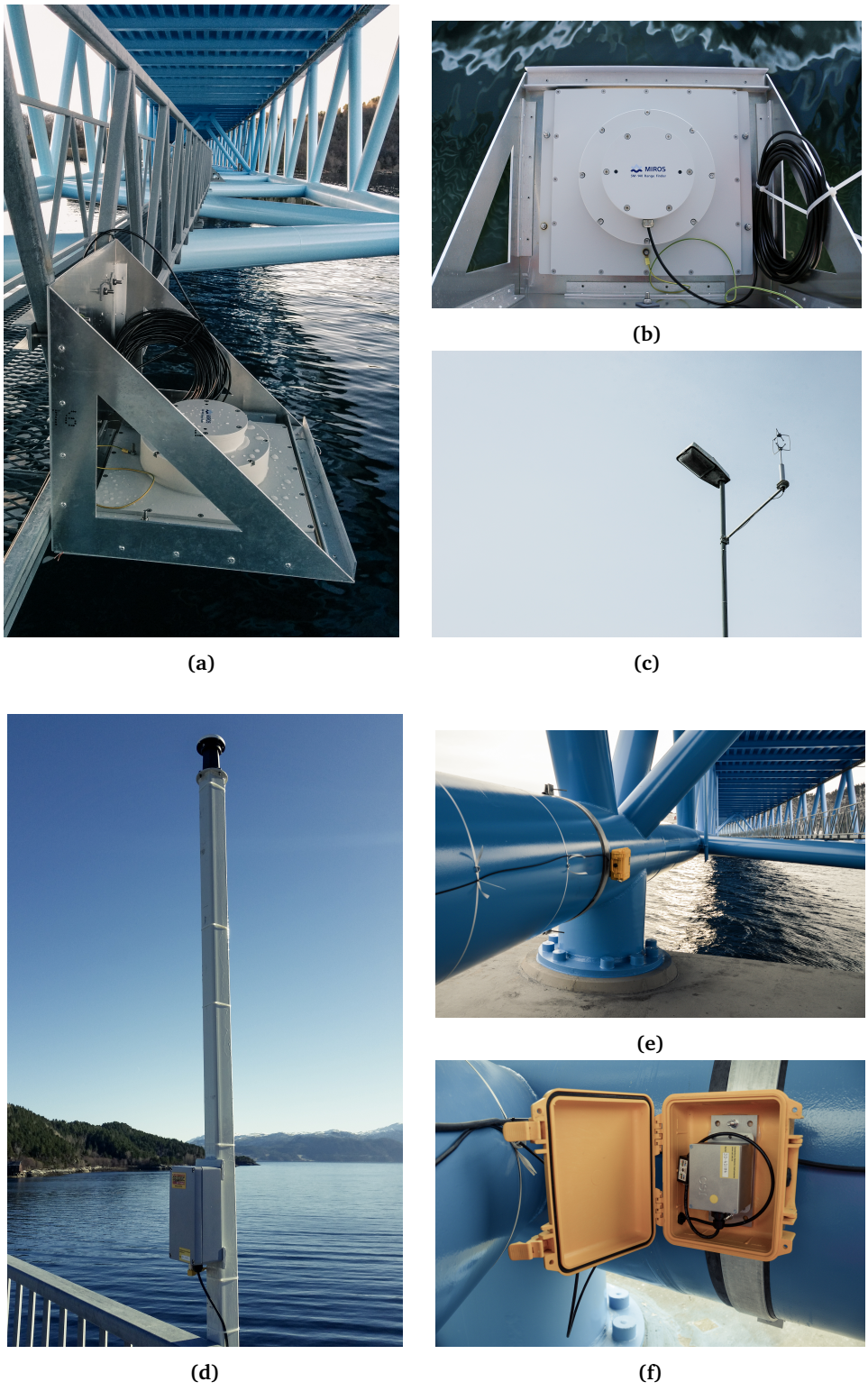

Figure 6. Photos of sensors. Photo: NTNU/K.A. Kvåle. (a)-(b) Miros SM-140 Range Finder, wave radar, (c) Gill Instruments WindMaster Pro anemometer, (d) Trimble RTK GNSS, displacement sensor, (e)-(f) Canterbury Seismic Instruments CUSP-3, triaxial accelerometer.

Figure 7. Damaged anemometer A3 needed to be changed during sensor layout revision *Main*.

1. No identical distance vectors.
2. Uniform distribution (direction and lengths) of distance vectors.
3. The smallest distance vector should be able to capture the highest frequency (shortest) waves of interest. This is ensured by letting at least one wave radar pair have distance below 0.25 of the shortest wave component considered. The shortest wave length can be calculated as $\lambda_{min} = \frac{2\pi}{\kappa_{max}} = \frac{2\pi g}{\omega_{max}^2}$. Here, κ_{max} is the wave number which, from the linear dispersion relation for deep water, is related to the circular frequency through $\kappa = \omega^2/g$.

The original layout directly fulfils guideline 1 from its circular pattern. However, neither guideline 2 nor 3 are fulfilled. The distance vectors are all close to being fully longitudinal, and many of them have equal lengths. Also, the largest peak frequency of interest is close to 1.6 rad/s, which implies that the shortest distance should be below 6 meters. The original (layout *Main*) and updated (layout *Alternative*) wave radar positions are depicted in Figure 8. The listed violations of the guidelines were drastically improved in the revised layout. Due to practical limitations, the updated layout is not strictly compliant to the listed guidelines neither. As indicated in Kvåle (2017) and demonstrated in Petersen et al. (2019), the updated sensor layout (Alternative) performs well with characterizing the directional waves for the relevant sea states at the site.

4 Data

The following section describes some crucial aspects concerning the data, such as the processing conducted and its structure. For the most part, this is in line with that reported in Fenerci et al. (2021) describing the data set obtained with a similar monitoring system on the Hardanger Bridge.

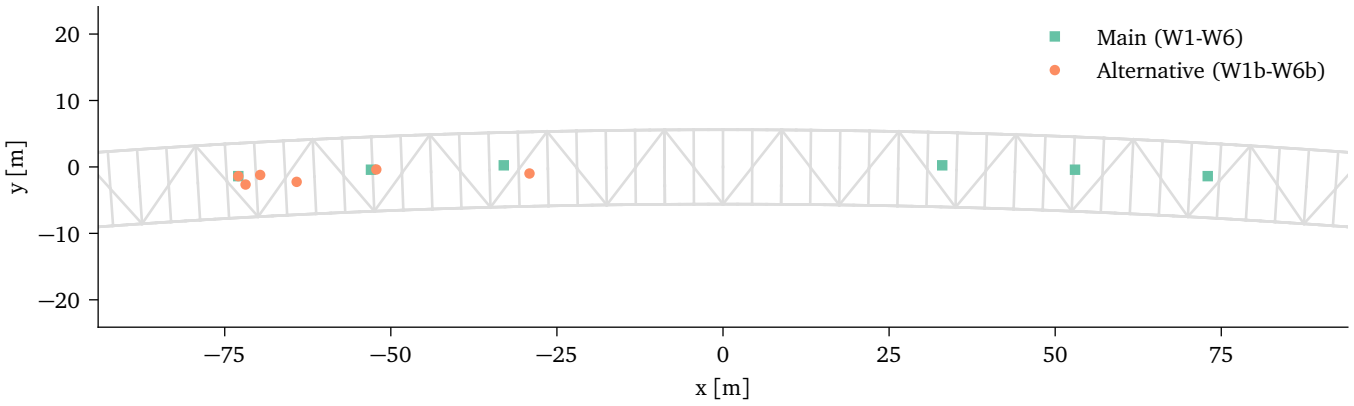

Figure 8. Old and new arrangement of wave radars, with shaded truss elements.

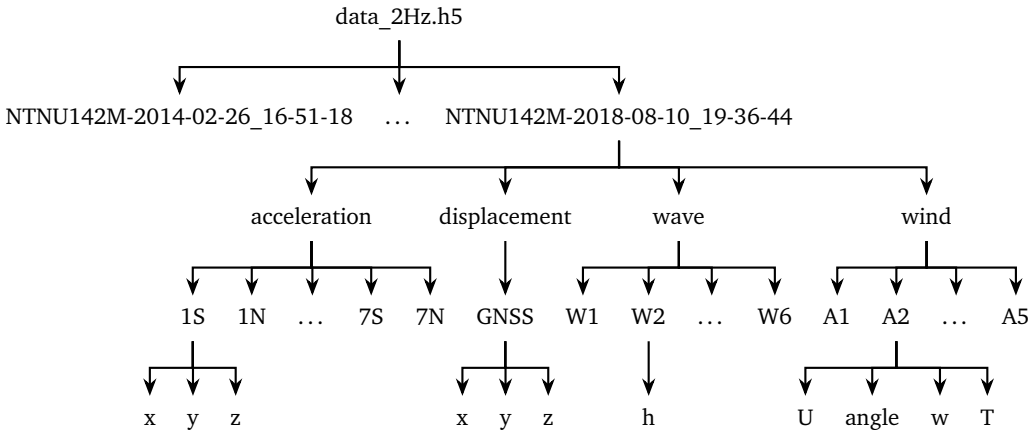

Figure 9. Hierachy of data set in h5-format.

4.1 Data format and hierachical structure

All recordings are collected in a single h5-file for each enforced sample rate. In the current database, the sample rates of 2 Hz and 10 Hz were used. However, for applications requiring higher sample rates, please contact the authors and we will attempt to provide data in higher rates. Note that the sensors themselves operate at other sampling frequencies, as indicated in Table 2.

We consider the HDF format very well suited for sharing. The hierarchical nature of the format ensures that the data are organized in a structured manner, ensuring a more intuitive usage, and consequently reduces the need for metadata describing the data structure. Furthermore, metadata are added in several of the levels of the hierarchy, to fully describe the data sets. Figure 9 depicts the structure of the data (2 Hz and 10 Hz versions share identical hierarchy and structure). Furthermore, to simplify the task of retrieving a useful time series for further analysis, some global statistics, i.e., mean values and standard deviations, are collected in a separate group called *.global_stats* at the root of each file. The hierarchy of the statistics group is given in Figure 10.

4.2 Metadata

Important metadata are distributed across different levels of the file hierarchy. This is depicted in Figure 11. For the most part, the metadata entries are self-explanatory. However, some of them would benefit from an elaboration.

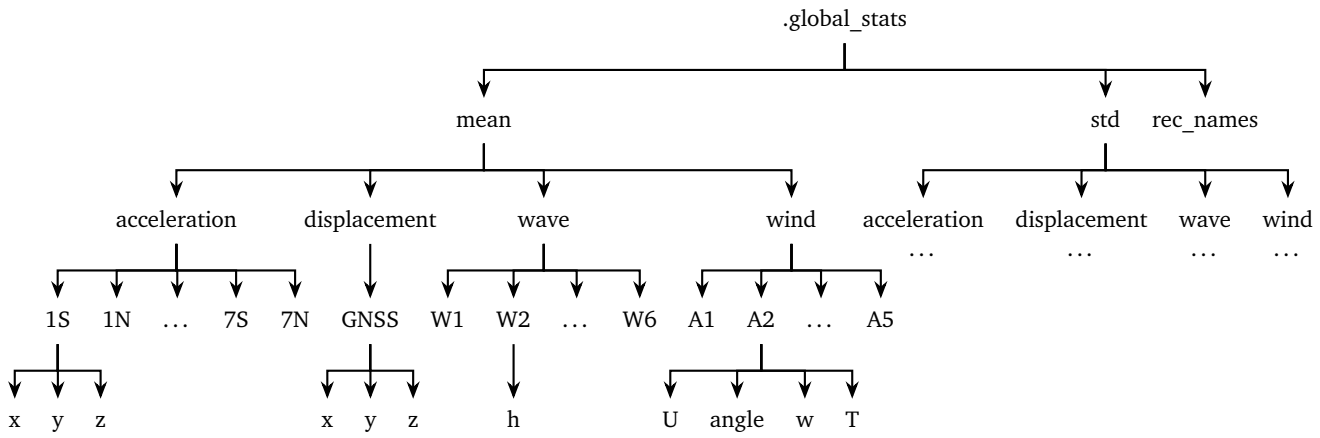

Figure 10. Hierachy of global statistics appended to h5-file.

Selected metadata entries are therefore described in Table 4.

4.3 Triggering schemes, recording lengths and naming convention

The monitoring system has been sensing continuously during the four-year period of the data set, but has only recorded data when triggered. The triggering schemes and recording durations have been varying during the campaign period. For most of the time, the system has been recording in 30-minute long time periods, triggered by a sensor reporting values exceeding some predefined threshold value. However, for some periods, the triggering has been continuous, meaning that each recording successively followed the previous one until manually stopped. Furthermore, some of the recordings are also shorter.

The recordings are named after their triggering time, using the following pattern: NTNU142M-YYYY-MM-DD_hh-mm-ss, where YYYY-MM-DD is the date, hh-mm-ss is the time based on a GMT+0 time schedule, and NTNU142M is the name of the main logger unit.

4.4 Processing

The data set is defined with respect to the global coordinate system (CSYS) depicted in Figure 4, whereas each sensor originally report data in their respective local CSYS. A transformation matrix $[\mathbf{T}]$ is used to transform the data from the local CSYS to the global CSYS. As described in the succeeding Section 4.2, this transformation matrix is provided as metadata for all sensors, as well as an description of the global CSYS. The transformation is applied in the following manner:

$$\{\mathbf{q}(t_k)\} = [\mathbf{T}]\{\bar{\mathbf{q}}(t_k)\} \tag{1}$$

where $\{\mathbf{q}(t_k)\} = [q_x, q_y, q_z]^T$ is the data quantity expressed in a global CSYS at time t_k, whereas $\{\bar{\mathbf{q}}(t_k)\}$ represents the corresponding local data. Each row in the 3-by-3 matrix $[\mathbf{T}]$ is simply the unit direction vectors describing the local axes for the sensor. In practice, the transformation is conducted by transforming the entire data matrix, containing the triaxial data for all time instances, in one operation:

$$[\mathbf{Q}] = \left([\mathbf{T}][\bar{\mathbf{Q}}]^T\right)^T \tag{2}$$

where $[\mathbf{Q}]$ and $[\bar{\mathbf{Q}}]$ are the data matrices with components stacked column-wise and time instances row-wise, represented in global CSYS and local CSYS, respectively.

The following steps of processing are conducted for all sensors:

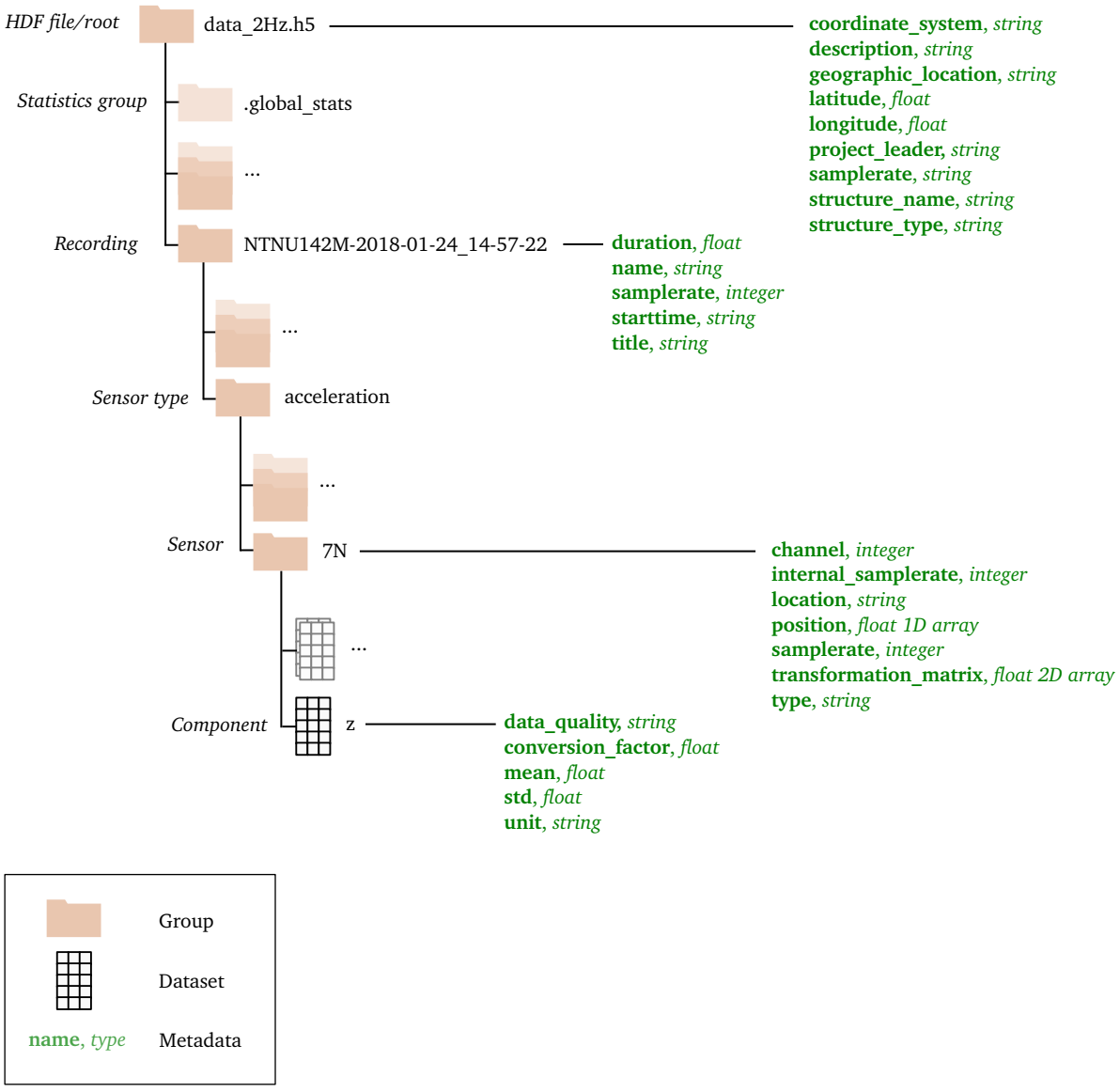

Figure 11. Metadata in HDF files.

Table 4. Description of selected metadata variables.

Hierarchy level	Name	Description
Project	*coordinate_system*	String describing the global coordinate system with words, including position of origin and the global axes directions.
	samplerate	The sample rate provided on the project level is given as a string as it is descriptive rather than a precise float number. Also, for some future projects, it might be relevant to gather data of several different sample rates in the same files.
Recording	*starttime*	String describing the date and time in GMT+0 that the recording was triggered. This has the structure **YYYY**-**MM**-**DD**T**hh**:**mm**:**ss**.
Sensor	*channel*	Channel for storing of data in raw data. Only used if accessing raw data are needed.
	location	String describing position of sensor.
	position	Array with coordinates of the sensor, with respect to the predefined global coordinate system.
	transformation_matrix	Transformation matrix (3x3 array) used to transform the sensor data to the global coordinate system. See Section 4.4 and specifically Equation 1. As described in the referred section, the rows of the matrix indicate the local axes of the sensor as mounted on the structure.
	type	Model name of the sensor.
Component	*data_quality*	String characterizing the quality of the data. This is established during the preprocessing of the data.
	conversion_factor	Conversion factor to establish data of specified unit. Not used for the Bergsøysund data, but included for future flexibility.
	unit	Unit of the data after the application of the conversion factor.

Table 5. Valid data ranges.

Sensor type	Component	Valid range	Type
Accelerometer	x,y,z	-2–2 g	Absolute value
Anemometer	U	0–50 m/s	Absolute value
	angle	-180–540°	Absolute value
	w	-50–50 m/s	Absolute value
	T	-50–50 m/s	Absolute value
GNSS displacement sensor	x,y,z	-2–2 m	Relative to mean value
Wave radar	h	3–5 m	Absolute (distance to water surface)

1. *Fixing corrupt data, interpolating and scoring data.* Data far outside some predefined valid ranges are removed, and filled by interpolated data. The valid ranges are defined separately for all sensor types. The applied valid ranges of the data from each sensor type are listed in Table 5. The same procedure is applied to data samples which are larger than five times the standard deviation of the corresponding time series. If the data from a component is constant for a time period above 0.5 seconds, the same procedure is carried out. Based on the amount of correction required during this step, all recordings are given a quality score: good (no correction required), acceptable (less than 10 seconds of data affected) or poor (more than 10 seconds affected). If the data are given the score *poor*, the entire data signal of the component is set to NaN (not a number), to avoid the analysis of that data causing erroneous results.

2. *Downsampling.* The downsampling is conducted using the MATLAB function `resample`, which lowpass filters the data prior to downsampling, to avoid aliasing.

3. *Transformation to global CSYS*. All three-dimensional data are in general transformed to a global CSYS by Equation 2. As the anemometer provides polar data, some special treatment of this is required. The wave radar provides 1D data of the vertical distance to the sea surface, and does thus not require any transformation.

The choice of sample rates 2 Hz and 10 Hz are supported by these two aspects: (i) the bridge is mainly excited by wind and waves which are both dominating at lower frequencies, and (ii) the natural frequencies of the first 20 modes are below 1 Hz. The lateral (y-direction) acceleration time series obtained by accelerometer 4S is depicted with its raw sampling rate and downsampled versions in Figure 12, from recording NTNU142M-2017-03-14_22-27-06. As expected, very high-frequent transient effects are not represented in the downsampled data; however, the wave- and wind-induced effects will be well described.

4.4.1 Special anemometer considerations

Due to the polar nature of the data output from the anemometers, the resulting local data has to be transformed to cartesian wind coordinates prior to transformation to the global coordinate system. Finally, the global cartesian data are transformed back to a polar format. Furthermore, traditional arithmetic means will provide misleading results when dealing with the measured wind angle. The same can be argued on other statistical quantities, such as standard deviations. Therefore, the statistical operations are applied to vectors representing the angular values, which are used to establish the final mean angles that are inserted in the database.

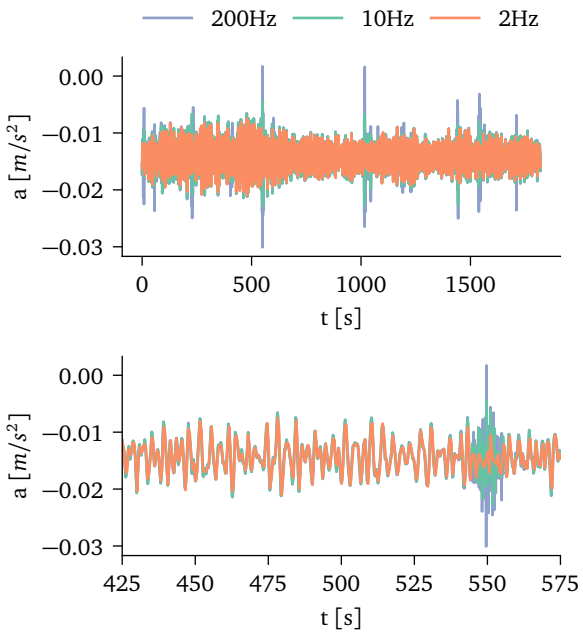

Figure 12. Time series of lateral component (y-direction) of accelerometer 4S.

4.5 Data examples

Figures 13 and 14 show the power-spectral density (PSD) estimates of the sea surface elevation and selected acceleration components, respectively, from a recording performed during relatively normal wave conditions. The vibrations are thus small and quite wide-banded. The harshest wave conditions during the campaign were observed December 30, 2015. The corresponding PSD estimates of wave elevation and selected acceleration components are shown in Figures 15 and 16, respectively. As the figures show, this excitation is far more narrow-banded and is dominated by modes near the peak frequency of the wave excitation. All PSD estimates are conducted on the 10-Hz data using Welch's method, with a 1024-samples-long Hanning window and a zero-padding factor of 4, implying 3×1024 zero samples for each FFT.

5 Open access database

The data are published in the open-access repository Zenodo under the Creative Commons license CC-BY 4.0 (Kvåle et al., 2022a). The data can be accessed with the following link: https://doi.org/10.5281/zenodo.5827293. Zenodo is an open-access repository developed under CERN's OpenAIRE program, stored in CERN Data Center. As the data set itself has both a DOI and Zenodo supports version DOIs, the data might be updated at some point. We will strive to retain the described structure of the data in any future version releases.

5.1 Python examples

Some useful functions for data import, processing and visualization are provided in the Python package `opyndata` on GitHub (Kvåle, 2022). The package will be updated and revised in the future, hopefully keeping core functionality backwards compatible. Please refer to the package documentation for more details about installation and usage.

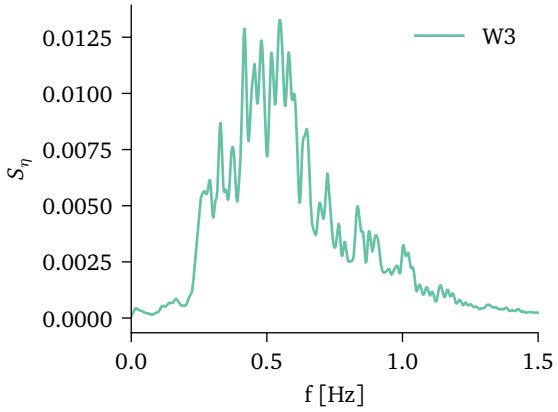

Figure 13. The PSD of sea surface elevation from wave radar W3, from recording NTNU142M-2017-03-14_22-27-06.

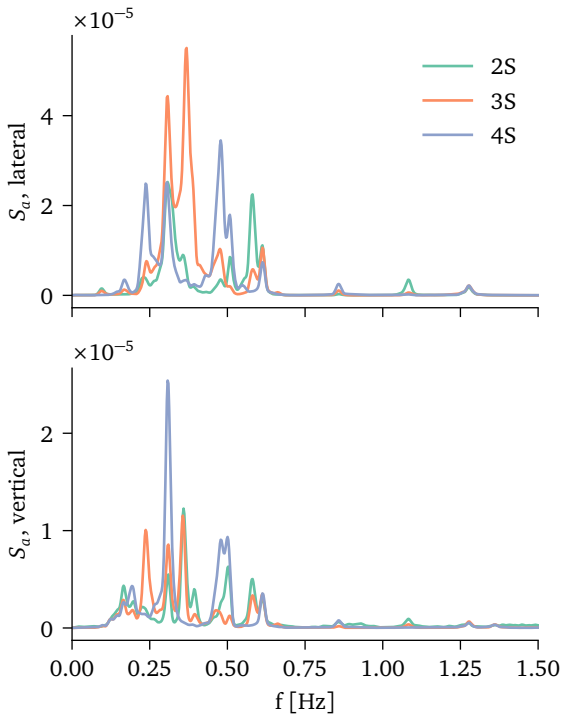

Figure 14. The PSD of lateral and vertical accelerations from accelerometers 2S, 3S and 4S, from recording NTNU142M-2017-03-14_22-27-06.

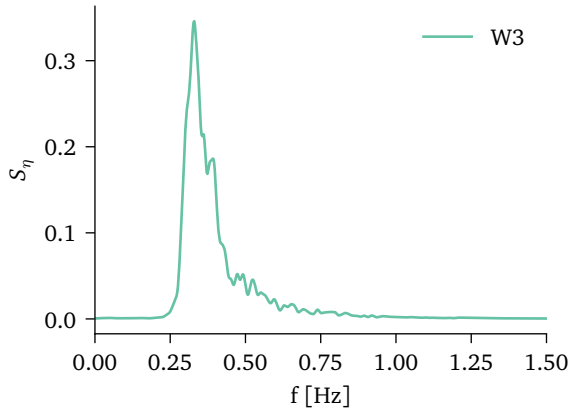

Figure 15. The PSD of sea surface elevation from wave radar W3, from recording NTNU142M-2015-12-30_03-20-21. This recording corresponds to the harshest waves observed during the campaign.

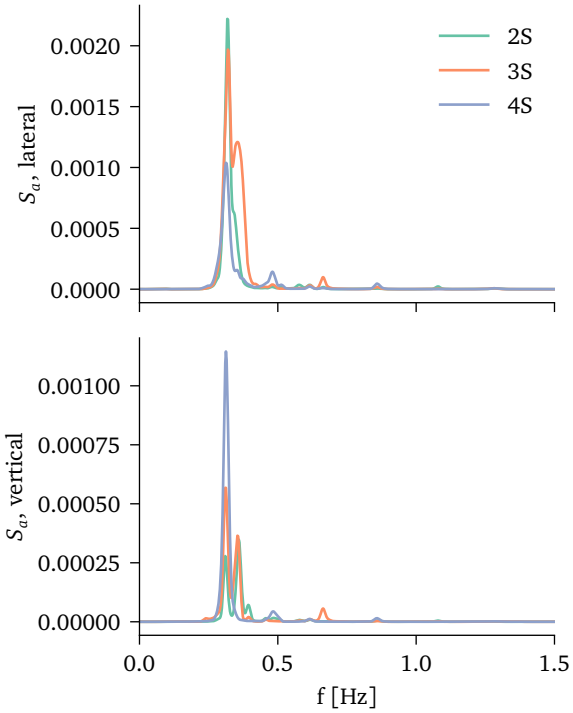

Figure 16. The PSD of lateral and vertical accelerations from accelerometers 2S, 3S and 4S, from recording NTNU142M-2015-12-30_03-20-21. This recording corresponds to the harshest waves observed during the campaign.

In the following sub-sections, some examples of import and visualization of the data set are provided for convenience. The examples are also published on the `opyndata` GitHub repository (Kvåle, 2022).

5.1.1 Load data set from single recording and visualize sensor positions

The code shown in Figure 17, also available in *example_single_rec.py* in `opyndata`, is run to create a sensor plot and import the data of a selected recording from the h5-file as a Pandas Dataframe object.

```
from opyndata.data_import import export_from_hdf
from opyndata.visualization import plot_sensors
import h5py
import plotly.io as pio

pio.renderers.default='browser'

# Define file and recordings
fname = 'data_2Hz.h5'
rec_name = 'NTNU142M-2017-03-14_22-27-06'

# Plot sensors
with h5py.File(fname, 'r') as hf:
    hf_rec = hf[rec_name]
    fig = plot_sensors(hf_rec, view_axis=2)
    fig.show()

# Choose components to import
comp_dict = {'wave': ['h'],
             'acceleration': ['x', 'y', 'z'],
             'wind': ['U']}

# Import recording from h5 file as Pandas dataframe
with h5py.File(fname, 'r') as hf:
    data_df = export_from_hdf(hf[rec_name], component_dict=
        comp_dict)
    data_df = data_df.set_index('t')    # set time as index
```

Figure 17. Example code to load single recording from h5 file.

The sensor plot is shown in Figure 18. The resulting Pandas Dataframe object is depicted in Figure 19.

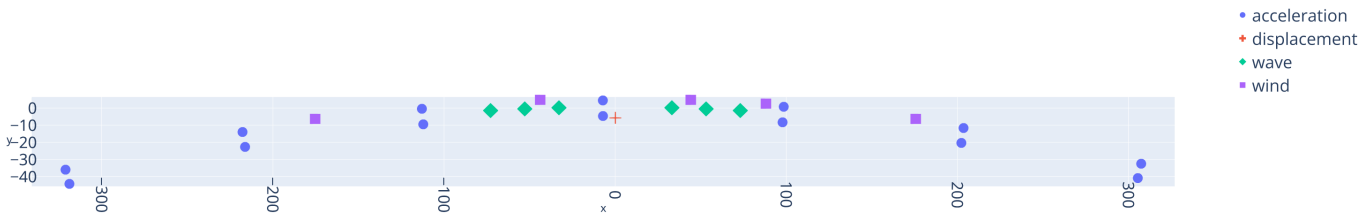

Figure 18. Resulting sensor position plot, based on metadata in h5-file. The plotting function is based on the `plotly` package.

```
In [13]: data_df
Out[13]:
                 1N/x      1N/y      1N/z  ...       A3/U       A4/U       A5/U
t                                          ...
0.000000    -0.007905  0.004950  0.006578  ...  13.869278  12.712683  14.593049
0.500135    -0.008379  0.005662  0.007062  ...  19.269735  16.723706  20.224925
1.000269    -0.008771  0.007042  0.007946  ...  17.010411  16.311568  20.195921
1.500404    -0.008432  0.005991  0.007348  ...  14.365299  17.823151  20.028311
2.000539    -0.007540  0.003182  0.006636  ...  15.028133  17.680238  19.545321
...               ...       ...       ...  ...        ...        ...        ...
1817.989461 -0.007382  0.004636  0.006542  ...  11.967637  13.074667   7.391795
1818.489596 -0.007418  0.004859  0.006112  ...  10.084129  12.951186   7.078698
1818.989731 -0.008067  0.007212  0.006316  ...  10.338453  12.938737   5.244156
1819.489865 -0.007614  0.005700  0.006916  ...  10.678658  14.856558   4.856929
1819.990000 -0.007157  0.004072  0.007203  ...   9.861242  10.529835   5.550638

[3640 rows x 53 columns]
```

Figure 19. Dataframe resulting from import code.

5.1.2 Browse data graphically in web browser

The code shown in Figure 20, also available in *visualize_h5_data.py* on `opyndata`, is run to create a dashboard to browse the h5-files.

```python
from opyndata import visualization

data_path = 'data_10Hz.h5'
app_setup = visualization.AppSetup(data_path=data_path)
app = app_setup.create_app()

server = app.server

# ------------ RUN SERVER -------------
if __name__ == '__main__':
    app.run_server(debug=False)
```

Figure 20. Example code to visualize h5 data.

This uses the `dash` Python package to host a local web page at http://127.0.0.1:8050/. By accessing this IP-address through a browser, a GUI appears, such that the data can be browsed in a graphical manner. Figure 21 depicts its appearance. The three sections show the statistical data, the data from the recording selected and the corresponding sensor layout. By providing this simple tool for browsing the data, it will hopefully become more available and accessible.

5.2 Numerical reduced-order model

To supplement the data, a reduced-order modal model can be found on the same repository as the data. This is based on the bridge model including the static restoring stiffness from buoyancy, but disregarding added mass and potential damping representing the hydrodynamic radiation forces. For more details on how this can be processed and included in a complete computational setup, please refer to Kvåle et al. (2015). The model is described by the following Numpy array variables, stored in *modal_model_bergsoysund.npz*:

- m (50-by-1): modal mass of 50 first modes
- omega_n (50-by-1): undamped circular natural frequency of 50 first modes

Figure 21. Graphical interface for browsing h5-files.

- phi (42-by-50): modal transformation matrix where mode shapes are stacked column-wise – degrees of freedom are given in a global CSYS and stacked in the order x, y, z, rotation about x, rotation about y, rotation about z, from pontoon 1 through 7
- coordinates (7-by-3): coordinates of the 7 pontoons for which the modal transformation matrix is given (the points refer to central point on the top of the pontoons)

6 Summary

In this data paper, we introduced and described a data set containing large amount of data retrieved from the Bergsøysund Bridge in Norway between the years 2014 and 2018. Also, the monitoring system used to collect the data is described. The data are available for free access under the CC-BY 4.0 license on Zenodo. The DOI corresponding to the data will be permanent, and if changes are made, the different versions of the data will be available under different version DOIs. Finally, by the usage of the Python package `opyndata` available on GitHub, the import and visualization of the data sets were exemplified, for convenience.

7 Data availability statement

Some or all data, models, or code generated or used during the study are available in a repository online in accordance with funder data retention policies. The data can be downloaded here: https://doi.org/10.5281/zenodo.5827293.

ACKNOWLEDGEMENTS

This research was conducted with financial support from the Norwegian Public Roads Administration. The authors gratefully acknowledge this support.

References

Fenerci, A., Andreas Kvåle, K., Wiig Petersen, Ø., Rønnquist, A., and Øiseth, O. (2021). "Data Set from Long-Term Wind and Acceleration Monitoring of the Hardanger Bridge." *Journal of Structural Engineering*, 147(5), 04721003.

Goda, Y. (1981). "Simulation in examination of directional resolution." *Proceedings of Directional Wave Spectra Applications*, 387–407.

Johnson, E. A., Lam, H. F., Katafygiotis, L. S., and Beck, J. L. (2004). "Phase i iasc-asce structural health monitoring benchmark problem using simulated data." *Journal of Engineering Mechanics*, 130(1), 3–15.

Kvåle, K. A. (2017). "Dynamic behaviour of floating bridges exposed to wave excitation. A numerical and experimental investigation." Ph.D. thesis, NTNU,

Kvåle, K. A. (2022). "OpyNDATA Python package." *Zenodo*. https://doi.org/10.5281/zenodo.5978357.

Kvåle, K. A., Fenerci, A., Petersen, Ø. W., Rønnquist, A., and Øiseth, O. (2022a). "Data set from long-term wave, wind and response monitoring of the Bergsøysund Bridge [Data set]." *Zenodo*. https://doi.org/10.5281/zenodo.5827293.

Kvåle, K. A., Fenerci, A., Petersen, Ø. W., Rønnquist, A., and Øiseth, O. (2022b). "Data set from long-term wind and acceleration monitoring of the Gjemnessund Bridge [Data set]." *Zenodo*. https://doi.org/10.5281/zenodo.5979694.

Kvåle, K. A. and Øiseth, O. (2017). "Structural monitoring of an end-supported pontoon bridge." *Marine Structures*, 52, 188–207.

Kvåle, K. A. and Øiseth, O. (2019). "Characterization of the Wave Field Around an Existing End-Supported Pontoon Bridge from Simulated Data." *Proceedings of the International Conference on Earthquake Engineering and Structural Dynamics*, R. Rupakhety, S. Olafsson, and B. Bessason, eds., Cham, Springer International Publishing, 345–359.

Kvåle, K. A. and Øiseth, O. (2021a). "Automated operational modal analysis of an end-supported pontoon bridge using covariance-driven stochastic subspace identification and a density-based hierarchical clustering algorithm." *Bridge Maintenance, Safety, Management, Life-Cycle Sustainability and Innovations*, CRC Press, 3041–3048.

Kvåle, K. A. and Øiseth, O. (2021b). "Dynamic Response of an End-Supported Pontoon Bridge due to Wave Excitation: Numerical Predictions versus Measurements." *Shock and Vibration*, 2021, 8842812.

Kvåle, K. A., Øiseth, O., and Rønnquist, A. (2017). "Operational modal analysis of an end-supported pontoon bridge." *Engineering Structures*, 148, 410–423.

Kvåle, K. A., Sigbjörnsson, R., and Øiseth, O. (2016). "Modelling the stochastic dynamic behaviour of a pontoon bridge: A case study." *Computers & Structures*, 165, 123–135.

Maeck, J. and De Roeck, G. (2003). "Description of Z24 benchmark." *Mechanical Systems and Signal Processing*, 17(1), 127–131.

Maes, K. and Lombaert, G. (2021). "Monitoring Railway Bridge KW51 Before, During, and After Retrofitting." *Journal of Bridge Engineering*, 26(3), 4721001.

Petersen, Ø. and Øiseth, O. (2017). "Sensitivity-based finite element model updating of a pontoon bridge." *Engineering Structures*, 150, 573–584.

Petersen, Ø., Øiseth, O., and Lourens, E. (2019). "Full-scale identification of the wave forces exerted on a floating bridge using inverse methods and directional wave spectrum estimation." *Mechanical Systems and Signal Processing*, 120, 708–726.

Petersen, Ø., Øiseth, O., Nord, T. S., and Lourens, E. (2018). "Estimation of the full-field dynamic response of a floating bridge using Kalman-type filtering algorithms." *Mechanical Systems and Signal Processing*, 107, 12–28.

Wernitz, S., Hofmeister, B., Jonscher, C., Grießmann, T., and Rolfes, R. (2021). "Dataset: LUMO - Leibniz Universtity Test Structure for Monitoring.